

# Conformal holographic Metasurface-Based Beamforming Antenna using a 3D-Printed Flexible Substrate

Praveen Kumar Sharma<sup>1</sup>, Aakash Bansal<sup>1</sup>, and Jae-Young Chung<sup>1</sup>

<sup>1</sup>Affiliation not available

April 01, 2024

# Conformal Holographic Metasurface-Based Beamforming Antenna using a 3D-Printed Flexible Substrate

Praveen Kumar Sharma, Aakash Bansal, *Member, IEEE*, and Jae-Young Chung, *Senior Member, IEEE*

**Abstract**—This paper presents the design of a holographic metasurface-based beamforming antenna. The metasurface, built on the holographic principle, showcases its transformative ability by converting an omnidirectional monopole into a highly directional antenna. Here, we present a holographic metasurface antenna designed on top of a novel 3D-printed substrate to maintain light-weight and achieve conformality. It is meticulously tailored for optimal performance at 15 GHz with precise beam at 60° while converting the omnidirectional pattern of the monopole to directional antenna offering gain of 13 dBi using a holographic metasurface. The results of the holographic metasurface antenna are verified with cylindrical bending confirming its flexibility.

**Index Terms**—Metasurface, holography, beamforming, antenna.

## I. INTRODUCTION

THE IMMINENT requirement for novel and flexible communication systems has increased in recent years [1], [2]. Several technical barriers need to be addressed for antenna designers to harness antennas for flexible communication systems. In the aforementioned types of applications, having an accessible, compact, flexible, and easily integrable antenna is desirable. It is therefore essential to adequately choose and implement a substrate in order to build an antenna with flexible properties. With the increase in demand for flexible electronics and evolution of printing technology, researchers have been looking into new substrate materials.

As recent studies show [3]–[5] that polymer-based substrates offer multiple advantages over rigid and paper-based substrates, they are becoming increasingly prominent in antenna applications. Polyimide (PI) and similar thin film substrates are gaining greater acceptance in antenna applications [6]–[9]. Thin film substrates lend multiple benefits owing to their distinctive

Manuscript received \_\_\_\_\_; revised \_\_\_\_\_; accepted \_\_\_\_\_; date of publication \_\_\_\_\_; date of current version \_\_\_\_\_. This research was supported by the Basic Science Research Program through the National Research Foundation of Korea (NRF) funded by the Ministry of Education (NRF- 2019R1A6A1A03032119). (Corresponding author: Prof Jae-Young Chung)

Dr Praveen Kumar Sharma is with Research Center for Electrical and Information Technology, Seoul National University of Science and Technology, Republic of Korea (impraveenkumarsharma@gmail.com)

Dr Aakash Bansal is with Wolfson School of Mechanical, Electrical, and Manufacturing Engineering, Loughborough University, UK (a.bansal@lboro.ac.uk).

Prof Jae-Young Chung is with Dept. of Electrical and Information Technology, Seoul National University of Science and Technology, Republic of Korea (jychung@seoultech.ac.kr).

attributes, that foster the development of light, portable, and compact electrical devices. Along with electrical and mechanical properties, such films can also be tailored to have new optical characteristics such as high reflectivity, interference effects, and anti-reflection coatings [10]–[12].

Manipulating electromagnetic waves in antenna design has become prominent with the evolution of metasurfaces. Such surfaces use 2D subwavelength elements and generate highly directed beams. With precise control of the phase distribution across the metasurface, beam steering can be achieved without physical change in antenna structure [13]–[15].

Furthermore, metasurfaces perform exceptionally well in polarization control, allowing antennas to comply with certain polarization specifications in communication systems as well as defense applications [16]–[18]. In addition, by suppressing undesired polarization components in the radiation pattern, metasurfaces improve antenna performance by lowering cross-polarization. Though metasurfaces offer excellent prospects for inventive antenna design, current researches are more focused on addressing practical implementation challenges, particularly at higher frequencies, in order to fully fulfill metasurfaces' potential for advancing antenna technology [19], [20].

Holographic metasurface-based beamforming antennas demonstrate substantial strides in antenna engineering. Their adeptness for precise modulating and flexion electromagnetic waves eventually led to intriguing applications for wireless systems for telecommunications, imaging systems, radar, and satellite communication. As research and development for metasurface technology persists, the aforementioned antennas are anticipated to play an integral role in future generations of sensors and wireless communication [21]–[23].

First introduced in 1970s [24], holographic antennas were used to attain the requisite radiation characteristics. Since then, with the advancements in fabrication techniques, the holographic metasurface has become a key interest for many researchers. Several advancements in holographic antennas using rigid substrates are readily available in literature. The designed metasurfaces on rigid substrates are quite appropriate for beam-forming applications, but not very suitable for conformal applications where the antennas are required to be attached to uneven surfaces. Such metasurfaces can be optimized for flexible substrates, making them suitable for real-life applications. Furthermore, for applications in the space industry, such antennas need to be lightweight. Additive manufacturing such as 3D-printing has been shown to be very

useful for RF applications and can be used to print such flexible substrates [25]–[27].

This paper aims at developing a novel flexible holographic metasurface antenna using a new lightweight 3D printed flexible substrate to convert a monopole antenna into a beamformed directional antenna. The stipulated paper has been organized into five sections. Section II discusses the design principle of holographic metasurface. Section III delivers an extensive explanation of the antenna design; Section IV unveils the results and discussions; and Section V wraps up the research as conclusion.

## II. DESIGN PRINCIPLE

In optical holography, the conjunction of two waves, the object wave,  $\Psi_{obj}$  and the reference wave,  $\Psi_{ref}$  results in an interference pattern. This interference pattern is utilized to scatter the reference wave and produce the intended object wave and can be defined as [28], [29],

$$(\Psi_{obj}\Psi_{ref}^*)\Psi_{ref} = \Psi_{obj}|\Psi_{ref}|^2 \quad (1)$$

An analogous approach can be leveraged to create holograms for radiofrequency (RF) applications. The requisite radiation characteristics serve as an object wave, and the feed monopole antenna is used as a source for the reference wave, or surface wave in this case. Knowing monopole antenna has a cylindrical wavefront, the reference wave can be defined as,

$$\Psi_{ref} = e^{-jkn_r d} \quad (2)$$

Here,  $d$  and  $n_r$  are radial distance and refractive index from the monopole feed, respectively. Now, assuming the desired radiated beam is pointing in the direction  $\theta$  in azimuth plane, the object wave can be articulated as,

$$\Psi_{obj} = e^{-j(kx \sin \theta + \varphi)} \quad (3)$$

Here, the arbitrary offset phase is  $\varphi$ . The surface impedance, ( $Z_s$ ) which act as an interference pattern can be expressed as,

$$Z_s(x, y) = j X_{avg} [1 + M \text{Re}(\Psi_{obj}\Psi_{ref}^*)] \quad (4)$$

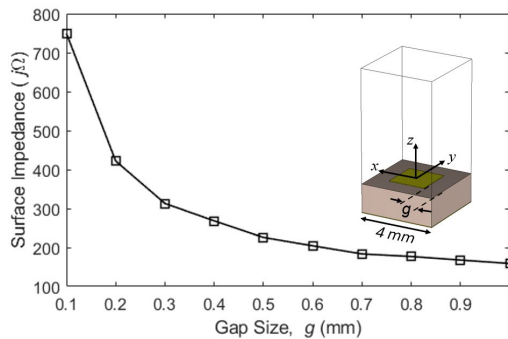


Figure 1: Change in surface impedance as a function of gap between unit-cell elements (Inset: unit-cell analysis within simulation).

In this case,  $M$  is the modulation depth and  $X_{avg}$  is the average surface impedance. The reference wave evolves into an object wave as it progresses along the holographic metasurface, and surface impedance calculations facilitate an analytical assessment of the requisite radiation characteristics. In order to simulate the surface impedance, a unit-cell with period 4 mm is employed using periodic boundary conditions, see Figure. 1. A

non-uniform structure can be designed by varying the geometric properties of the unit-cell. The impedance of the unit-cell is determined with change in gap size,  $g$  varying from 0.1 mm to 1 mm, see Figure 1. The surface impedance for the unit-cell is calculated using the method described in [30], and is found to spans from  $j749 \Omega$  to  $j160 \Omega$  at 15 GHz with change in gap size, whose least square fit can be obtained with the help of MATLAB.

The refractive index ( $n_r$ ) for the bound surface wave is expressed as:

$$n_r = \frac{c}{v_{ph}} = \frac{k_w c}{\omega_e} \quad (5)$$

Here,  $v_{ph}$  is the phase velocity,  $c$  is the speed of light and  $k_w$  is the wave vector of the surface wave. For a given phase offset,  $\varphi$  and unit cell dimension,  $u$ , the eigen frequency,  $\omega_e$  can be determined using the eigen mode solver of CST. The phase offset is expressed as,

$$\varphi = k_w u \quad (6)$$

Using this, the relative refractive index profile can be evaluated easily. The effective surface impedance is determined using,

$$Z_s = \frac{Z_0}{1 - n_r^2} \quad (7)$$

## III. ANTENNA DESIGN

### A. Antenna Schematic

The antenna design is made up of four layers: (i) metasurface layer on top; (ii) thin film layer with adhesive; (iii) 3D-printed substrate; and (iv) ground layer, see Figure 2(a). The top holographic metasurface layer is made up of copper and is designed based on the theory provided in Section II, and is designed for a substrate of relative permittivity,  $\epsilon_r = 2.2$  and height,  $h_s = 1.6$  mm. The top metasurface layer is bonded with the 3D-printed substrate using a GTS Mylar thin film of relative permittivity,  $\epsilon_r = 3.5$ , loss tangent,  $\tan \delta = 0.001$  and thickness,  $h_g = 30 \mu\text{m}$ . The antenna is fed using a monopole element of height,  $h_p = 3.30$  mm which serves as the source of the reference wave. The antenna design and geometric parameters are shown in Figure 2(b).

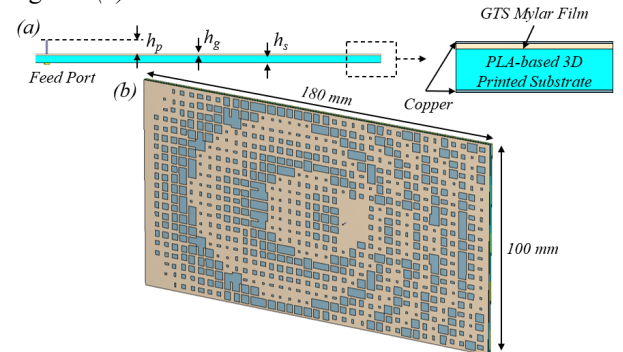


Figure 2: (a) Side view of the antenna design showing the four layers of copper, GTS Mylar film and 3D-printed substrate; (b) Orthogonal view of the holographic metasurface layer on top.

### B. 3D-Printed Substrate Design

The substrate design is the key to achieving flexibility within

the proposed holographic antenna design. Here, we use a white polylactic acid (PLA) thermoplastic material that offers a relative permittivity,  $\epsilon_r = 2.7$  and loss tangent,  $\tan \delta = 0.004$  at 15 GHz [26], [31]. The substrate is a 2D array of a 10 mm  $\times$  10 mm unit-cell with a hole of diameter,  $d_h = 7.5$  mm, see Figure 3(a). The introduction of hole ensures 60% of PLA material and 40% air-gap within the unit-cell and was characterized in CST Microwave Studio. The equivalent relative permittivity of such a substrate is  $\epsilon_e = 2.2$  and was confirmed using split post dielectric resonator method [32]. The printed height of the substrate was 1.6 mm  $\pm$  0.2 mm and is shown in Figure 3(b).

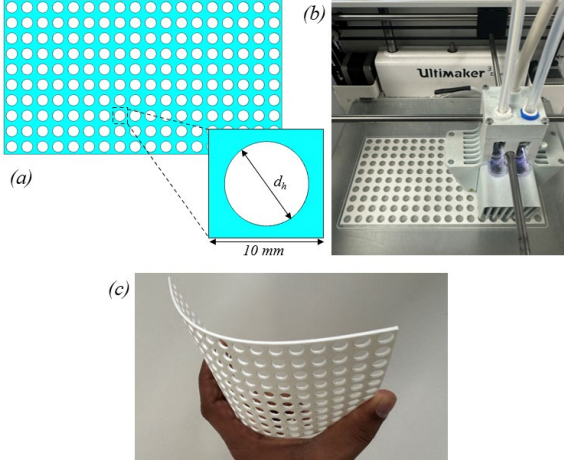


Figure 3: (a) Simulated substrate design within CST Environment; (b) 3D-printing of the substrate on an Ultimaker 3 printer; (c) final fabricated substrate easily conformed in hand.

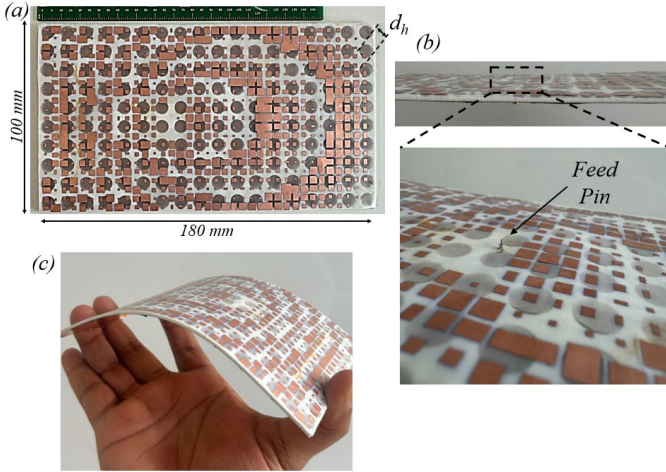


Figure 4: (a) Top and (b) side view of the fabricated antenna design; (c) the antenna design conformed in hand demonstrated flexibility.

C. Fabrication

The final fabricated antenna in planar and conformal forms are shown in Figure 4. The top layer is fabricated on a GTS Mylar sheet and then stuck on top of the substrate using a thin layer of generic adhesive. The ground plane of the antenna is created using copper tape. An SSMA connector is soldered on the ground plane and a tin wire is soldered on top of the connector to achieve the 3.30 mm tall monopole feed source. The fabricated antenna weighs 48 grams in total. Here, the 3D printed substrate was 25 grams.

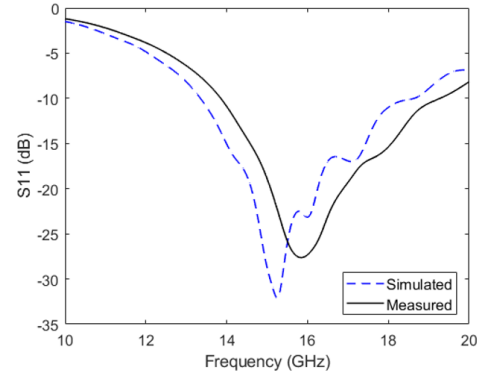


Figure 5: Simulated and measured  $S_{11}$  for the holographic metasurface antenna.

IV. PARAMETRIC ANALYSIS AND MEASURED RESULTS

A. Measured Results for Flat Design

The antenna was simulated using CST Microwave Studio. The simulated and measured  $S_{11}$  for the antenna is shown in Figure 5. The antenna has a measured resonant frequency of 15.5 GHz while the simulated resonant frequency is 15 GHz. The slight shift in frequency band is believed to be because of human error during the fabrication process. Besides, the measured  $S_{11}$  is found to be in line with that of simulations. The antenna shows a 10-dB bandwidth of approximately 14 to 19 GHz, however, the maximum gain and directionality is achieved at approximately 15 GHz because of the holographic metasurface.

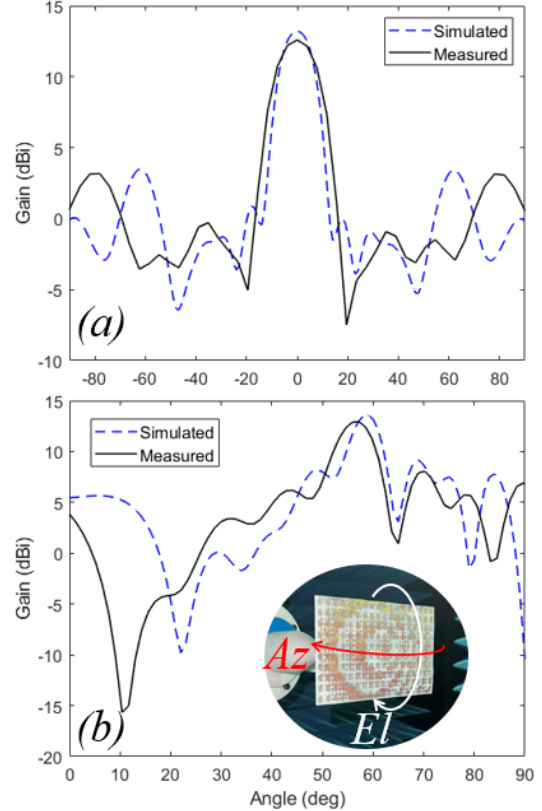


Figure 6: Simulated and measured radiation pattern of the antenna at 15 GHz in (a) elevation and (b) azimuth plane. Inset: fabricated antenna inside the anechoic chamber.

The simulated and measured gain patterns of the antenna for planar design at 15 GHz are shown in Figure 6. The antenna had a measured gain of 13 dBi with beam pointing angle of  $57^\circ$  in the azimuth plane. The measured results are very close to that of simulations. The side lobe levels (SLL) are maintained below 8 dB throughout the frequency band. The cross-polarized results were below -25 dB and hence, are not included here for brevity. The measured gain of the antenna over frequency is shown in Figure 7.

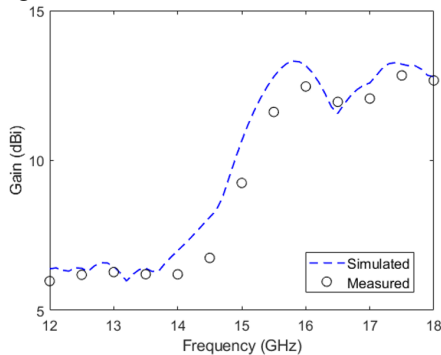


Figure 7: Simulated and measured gain as a function of frequency for the holographic metasurface antenna.

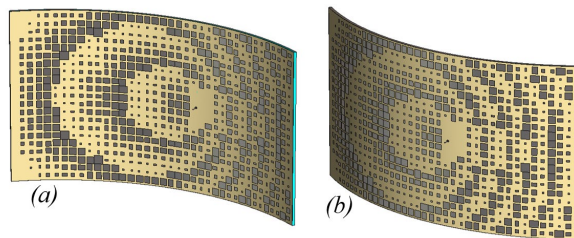


Figure 8: (a) Concave and (b) convex cylindrically bent holographic metasurface antennas with a bend radius of 150 mm.

**B. Measured Results for Conformed Design**

One of the key novelties of the proposed holographic metasurface antenna is its flexible structure which can easily be bent. The bending is done in cylindrical form along the long edge of the antenna structure and both concave and convex bends were considered within simulation, see Figure 8. However, as the bend radius for concave structure was reduced the E-field starts to interfere destructively, damaging the directional beam and hence, is not considered in this study.

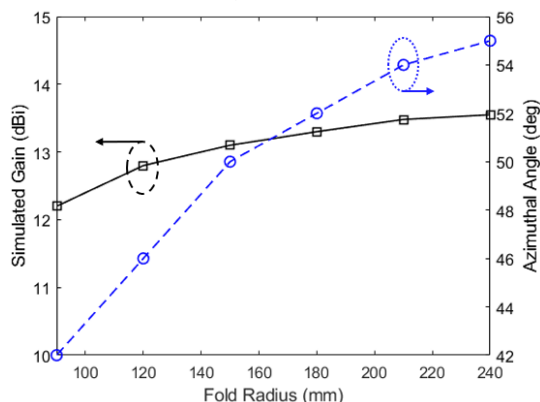


Figure 9: Simulated gain (left, solid black) and azimuthal beam-pointing angle (right, dashed blue) as a function of convex fold radius.

The antenna was bent convexly (as shown in Figure 8(b)) for a radius of 90 mm to 240 mm at 30 mm intervals. The simulated change in gain and beam-pointing angle in the azimuthal direction with the change in bend radius is shown in Figure 9. Two of these cases were verified within measurements with a bend radius of 150 mm and 210 mm. The measured radiation patterns for the two convexly bent configurations compared with the flat structure is shown in Figure 10. With the reduction in the bend radius, the gain of the antenna starts to reduce. This is because the holographic metasurface was designed for a planar surface, and degradation is introduced within the structure with bending. However, the gain reduced by only 1.4 dB when it is bent from flat surface to a radius of 90 mm, confirming the antenna is still suitable for conformal applications.

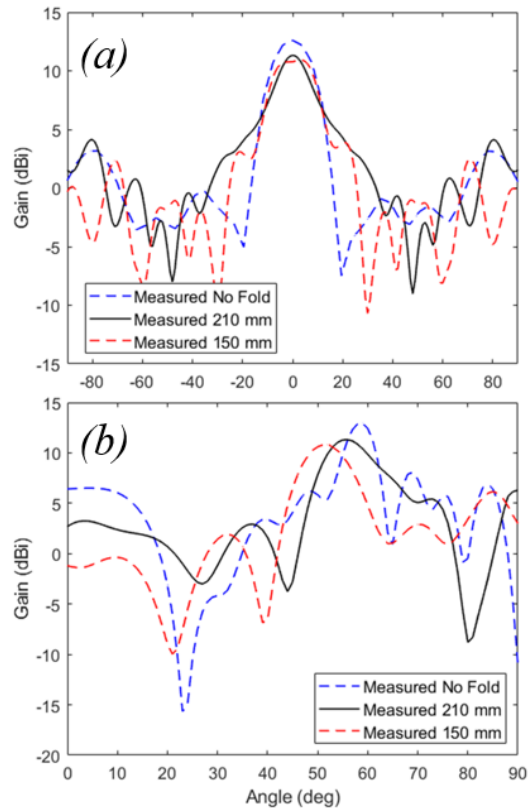


Figure 10: Measured convexly folded holographic metasurface antenna compared with flat surface in (a) elevation and (b) azimuth plane.

**V. CONCLUSION**

This paper presented a holographic metasurface antenna on a new 3D-printed substrate for flexibility. The proposed antenna offers a novel approach to achieve precise beam control using holography and offers a gain greater than 12 dBi across the operating frequency band. The proposed process can be repeated to change the beam angle to any desired location. The 3D-printed antenna weighed a total of 48 grams, making the system extremely light and suitable for space applications. The convex bending of the antenna shows slight degradation in the performance with a drop of 1.4 dB in gain and  $18^\circ$  in azimuthal beam-pointing angle in the worst-case scenario, making it still suitable for both terrestrial and non-terrestrial applications.

## ACKNOWLEDGEMENT

This research was supported by the Royal Academy of Engineering, the Office of the Chief Science Adviser for National Security under the UK Intelligence Community Postdoctoral Research Fellowships programme.

## REFERENCES

- [1] T. S. Rappaport *et al.*, "Millimeter wave mobile communications for 5G cellular: It will work!," *IEEE Access*, vol. 1, pp. 335–349, 2013, doi: 10.1109/ACCESS.2013.2260813.
- [2] A. Bansal, C. Panagamuwa, and W. Whittow, "Millimeter-Wave Beam Steerable Slot Array Antenna Using an Inter-Digitated Capacitor Based Corrugated SIW," *IEEE Trans. Antennas Propag.*, vol. 70, no. 12, pp. 11761–11770, 2022, doi: 10.1109/TAP.2022.3211013.
- [3] P. K. Sharma and J. Y. Chung, "Poly-flex-antennas: Application of polymer substrates in flexible antennas," *Express Polym. Lett.*, vol. 18, no. 4, pp. 371–390, 2024, doi: 10.3144/expresspolymlett.2024.28.
- [4] P. K. Sharma and J. Y. Chung, "Evaluation of Polydimethylsiloxane (PDMS) as a Substrate for the Realization of Flexible/Wearable Antennas and Sensors," *Micromachines*, vol. 14, no. 4, pp. 1–14, 2023, doi: 10.3390/mi14040735.
- [5] P. K. Sharma and J. Y. Chung, "Application of polydimethylsiloxane (PDMS) as a flexible substrate for wireless body and local area network antenna with CSRR integration," *Express Polym. Lett.*, vol. 17, no. 7, pp. 759–770, 2023, doi: 10.3144/expresspolymlett.2023.56.
- [6] O. R. Alobaidi, P. Chelvanathan, S. K. Tiong, B. Bais, M. A. Uzzaman, and N. Amin, "Transparent Antenna for Green Communication Feature: A Systematic Review on Taxonomy Analysis, Open Challenges, Motivations, Future Directions and Recommendations," *IEEE Access*, vol. 10, pp. 12286–12321, 2022, doi: 10.1109/ACCESS.2020.3044435.
- [7] D. N. Dao and J. Y. Chung, "A Miniaturized Thin-Film UWB Monopole Antenna Implemented with High-Dk Adhesive," *Electron.*, vol. 12, no. 16, 2023, doi: 10.3390/electronics12163445.
- [8] A. S. M. Sayem, A. Lalbakhsh, K. P. Esselle, J. L. Buckley, B. O'Flynn, and R. B. V. B. Simorangkir, "Flexible Transparent Antennas: Advancements, Challenges, and Prospects," *IEEE Open J. Antennas Propag.*, vol. 3, no. September, pp. 1109–1133, 2022, doi: 10.1109/OJAP.2022.3206909.
- [9] U. Pandey, P. Singh, N. P. Gupta, R. Singh, and A. Bansal, "Wideband leaky-wave antenna with dumbbell-shaped slots on substrate integrated waveguides with twisted corrugations," *Electron. Lett.*, vol. 59, no. 20, pp. 3–5, 2023, doi: 10.1049/el12.12991.
- [10] Y. Liu, Z. L. Wang, D. Y. Cang, J. S. Gong, and H. W. Qu, "A polyimide-based flexible monopole antenna," *J. Mater. Sci. Mater. Electron.*, vol. 33, no. 3, pp. 1686–1702, 2022, doi: 10.1007/s10854-022-07725-9.
- [11] Z. He, X. Lin, X. Yang, and C. Li, "A Flexible Microwave Ablation Antenna for Lung Cancer Treatment," *IEEE Antennas Wirel. Propag. Lett.*, vol. 22, no. 12, pp. 3147–3151, 2023, doi: 10.1109/LAWP.2023.3312147.
- [12] Z. P. Chen, Z. G. Liu, L. Ju, and W. B. Lu, "Beam scanning conformal antenna array with planar integrated phase shifter based on graphene," *J. Mater. Sci. Mater. Electron.*, vol. 33, no. 17, pp. 14032–14042, 2022, doi: 10.1007/s10854-022-08334-2.
- [13] S. Abulgasem, F. Tubbal, R. Raad, P. I. Theoharis, S. Lu, and S. Iranmanesh, "Antenna Designs for CubeSats: A Review," *IEEE Access*, vol. 9, pp. 45289–45324, 2021, doi: 10.1109/ACCESS.2021.3066632.
- [14] G. Oliveri, D. H. Werner, and A. Massa, "Reconfigurable electromagnetics through metamaterials—a review," *Proc. IEEE*, vol. 103, no. 7, pp. 1034–1056, Jul. 2015, doi: 10.1109/JPROC.2015.2394292.
- [15] M. Bodehou, E. Martini, S. Maci, I. Huynen, and C. Craeye, "Multibeam and Beam Scanning with Modulated Metasurfaces," *IEEE Trans. Antennas Propag.*, vol. 68, no. 3, pp. 1273–1281, 2020, doi: 10.1109/TAP.2019.2944554.
- [16] A. Bansal and W. G. Whittow, "Orbital Angular Momentum Beam Antenna Systems for Wireless Communications – A Brief Review," *2023 9th Int. Conf. Signal Process. Commun.*, pp. 125–128, 2023, doi: 10.1109/ICSC60394.2023.10441368.
- [17] M. K. T. Al-nuaimi, W. Hong, and W. G. Whittow, "Nature-inspired orbital angular momentum beam generator using aperiodic metasurface," *J. Phys. D: Appl. Phys.*, vol. 54, pp. 1–7, 2021.
- [18] J. Jin *et al.*, "Generation and detection of orbital angular momentum via metasurface," *Sci. Rep.*, vol. 6, Apr. 2016, doi: 10.1038/srep24286.
- [19] S. Dakhli, J. M. Floc'h, M. Aseeri, A. Mersani, and H. Rmili, "Design of Compact and Superdirective Metamaterial-Inspired Two- and Three-Elements Antenna Arrays," *J. Electromagn. Eng. Sci.*, vol. 23, no. 4, pp. 362–368, 2023, doi: 10.26866/jees.2023.4.r.179.
- [20] A. Bansal and W. Whittow, "Figuring out Impaired Reconfigurable Intelligent Surfaces," *TechRxiv Prepr.*, 2024, doi: 10.36227/techrxiv.171051649.95959056/v1.
- [21] W. Wan, J. Gao, and X. Yang, "Metasurface Holograms for Holographic Imaging," *Adv. Opt. Mater.*, vol. 5, no. 21, pp. 1–14, 2017, doi: 10.1002/adom.201700541.
- [22] D. Kampouridou and A. Feresidis, "Tunable Multibeam Holographic Metasurface Antenna," *IEEE Antennas Wirel. Propag. Lett.*, vol. 21, no. 11, pp. 2264–2267, 2022, doi: 10.1109/LAWP.2022.3192977.
- [23] Y. Wang, Q. Feng, X. Kong, H. Liu, J. Han, and L. Li, "Multi-Feed Beam-Switchable Cylindrical Conformal Holographic Metasurface Antenna," *IEEE Antennas Wirel. Propag. Lett.*, vol. 23, no. 3, pp. 970–974, 2023, doi: 10.1109/LAWP.2023.3340682.
- [24] P. Checcacci, V. Russo, and A. Scheggi, "Holographic antennas," *IEEE Trans. Antennas Propag.*, vol. 18, no. 6, pp. 811–813, Nov. 1970, doi: 10.1109/TAP.1970.1139788.
- [25] T. Whittaker, S. Zhang, C. Stevens, A. Powell, J. C. Vardaxoglou, and W. G. Whittow, "3D Printing Materials and Techniques for Antennas and Metamaterials," *IEEE Antennas Propag. Mag.*, pp. 2–12, 2022, doi: 10.1109/MAP.2022.3229298.
- [26] A. Bansal, C. J. Panagamuwa, and W. Whittow, "Novel Design Methodology for 3D-Printed Lenses for Travelling Wave Antennas," *IEEE Open J. Antennas Propag.*, vol. 4, no. January, pp. 196–206, 2023, doi: 10.1109/OJAP.2023.3243408.
- [27] A. Bansal, E. Mellios, H. Nagi, P. Febvre, and W. G. Whittow, "Two-Dimensional Beam-Steering Lens Antenna with Fast Inter-Beam Handover for PNT and Data Services for Satellite Communications on the Move," *TechRxiv Prepr.*, 2023, doi: <https://doi.org/10.36227/techrxiv.24157410.v1>.
- [28] A. Araghi, M. Khalily, P. Xiao, and R. Tafazolli, "Holographic-Based Leaky-Wave Structures: Transformation of Guided Waves to Leaky Waves," *IEEE Microw. Mag.*, vol. 22, no. 6, pp. 49–63, 2021, doi: 10.1109/MMM.2021.3064118.
- [29] N. A. Eltersy, H. A. Malhat, and S. H. Zainud-Deen, "Dual-beam Conformal Hologram Metasurface Leaky Wave Antenna Based On Surface Impedance Modulation," *Natl. Radio Sci. Conf. NRSC, Proc.*, vol. 2023-May, no. Nrsc, pp. 9–16, 2023, doi: 10.1109/NRSC58893.2023.10152886.
- [30] B. H. Fong, J. S. Colburn, J. J. Ottusch, J. L. Visher, and D. F. Sievenpiper, "Scalar and tensor holographic artificial impedance surfaces," *IEEE Trans. Antennas Propag.*, vol. 58, no. 10, pp. 3212–3221, 2010, doi: 10.1109/TAP.2010.2055812.
- [31] A. Bansal, H. Nagi, P. Febvre, and W. Whittow, "Bespoke Luneburg Lens for Two-Dimensional Beam-Steering Antennas for SatComms on the Move," *IEEE Int. Symp. Antennas Propag. Usn. Radio Sci. Meet.*, pp. 733–734, 2023, doi: 10.1109/USNC-URSI52151.2023.10238014.
- [32] C. K. Lee *et al.*, "Evaluation of microwave characterization methods for additively manufactured materials," *Designs*, vol. 3, no. 4, pp. 1–17, 2019, doi: 10.3390/designs3040047.